Gear rotation caused by self-propelling eccentric particles

Jincheng Gao,[1] Lin Liu,[1] Bin Tang,[1] Zequn Shi,[1] Huishu Li,[2] Tianhui Zhang,[1,*] Kang Chen,[1,†] and Wen-de Tian[1,‡]

[1]*Center for Soft Condensed Matter Physics & Interdisciplinary Research, School of Physical Science and Technology, Soochow University, Suzhou 215006, People's Republic of China*

[2]*School of Information Technology Suzhou Institute of Trade & Commerce, 287 Xuefu Road, Huqiu district, Suzhou 215009, People's Republic of China*

(Received 10 August 2025; revised 5 December 2025; accepted 8 January 2026; published 23 January 2026)

Extraction of useful work from the chaotic environments remains a captivating challenge. A gear in the bath of self-propelling eccentric particles is investigated by computer simulation. We find that the asymmetrical gear can rotate in a specific direction, with the angular speed first increasing and then decreasing as the eccentricity increases. Besides, a machine-learning model is trained to predict the angular speeds and the optimal one. Additionally, we observe that the directional rotation of a symmetric gear depends on the particle-area fraction, the persistence length of motion, and the eccentricity. Eccentricity is not conducive to the rotation of a symmetric gear, but a small degree of eccentricity can help increase the angular speed of the gear. There exist two mechanisms working for gear rotation at low eccentricity of particles: edge alignment with corner trapping and biased trapping with positive feedback. These insights suggest the tunable particle-level parameter, eccentricity, offers a promising strategy to regulate and optimize gear rotation.

DOI: 10.1103/njcd-mc48

I. INTRODUCTION

Extraction of useful work from the chaotic environments of molecules or particles remains a captivating issue for scientists, because it has immense potential application in biological systems and industry [1]. In equilibrium state, it is prohibited by the laws of thermodynamics due to the nonexistence of Maxwell demon [2]. It has been acknowledged that, to rectify a thermal system, both the time-reversal and/or spatial-inversion symmetries of the system must be broken [1]. Thus, the input of energy from either internal or external sources is required. Active-matter systems provide the possibility to realize the so-called "ratchet effect" [3]. The self-propulsion of active units intrinsically breaks time-reversal symmetry [4–7], whereas the broken spatial symmetry can be achieved by using asymmetrical structures. It was manifested by experiments with different types of active baths [3,8–11]. For example, Leonardo *et al.* [2] and Sokolov *et al.* [3] used bacteria to drive the directed rotation of submillimeter gears with asymmetrical teeth. The similar phenomena were also found in the artificial microswimmers systems, such as active Janus particles [12] and vibrated granular rods [8]. Net rotation of gears is caused by the momentum transfer from the self-propelling rodlike agents to gears. Gear asymmetry leads to a preferred rotation to one side than the other [10] due to agents accumulating in the corners of the gear and generating a net torque.

Theoretically, an asymmetrical gear in an active Brownian-particles (ABPs) bath was systematically investigated by Xu *et al.* [9]. They found the direction of rotation is determined by the asymmetry of the gear and the persistence length of active particles. At certain parameters (the self-propulsion speed, the rotation-diffusion coefficient, and the packing fraction of active particles), the gear can reversely rotate [9]. Although the unidirectional rotation of a symmetric gear in the bath of active units was not reported by experiments, it was deeply discussed by computer simulations [13–15]. Wang *et al.* [13] identified a spontaneous unidirectional rotation of a symmetric gear driven by spherical active Brownian particles. The mechanism is that gear rotation and induced-biased trapping of incident ABPs form a positive feedback loop that sustains the unidirectional rotation. Directed rotations of a symmetric gear driven by active chiral particles (ACPs) [14] or visual-perception-dependent particles (VPDPs) [15] were also detected recently, with different mechanisms. In the system of ACPs, the directed rotation results from the chirality-induced torque. While in the bath of VPDPs, the coupling of nonreciprocity and visual misalignment allows VPDPs to form clusters with persistent swirling, causing the directed rotation of gears. Hence, the type of active particles plays a critical role in the gear rotation. These studies have primarily focused on elucidating the underlying mechanisms responsible for the directed rotation of gears in different active baths. Less attention has been paid to enhancing the efficiency of torque generation. In particular, strategies for systematically tuning particle-level parameters to optimize the transfer of active momentum to the gear remain largely unexplored. Introducing controllable parameters—such as activity strength or sensory alignment—at the level of individual particles may offer a promising route to regulate and improve the rotational efficiency of gears.

Recently, self-propelling eccentric particles (SPEPs) were fabricated [16]. Particle eccentricity originates from the deviation between the geometric center (GC) and the center of mass

[*]Contact author: zhangtianhui@suda.edu.cn
[†]Contact author: kangchen@suda.edu.cn
[‡]Contact author: tianwende@suda.edu.cn

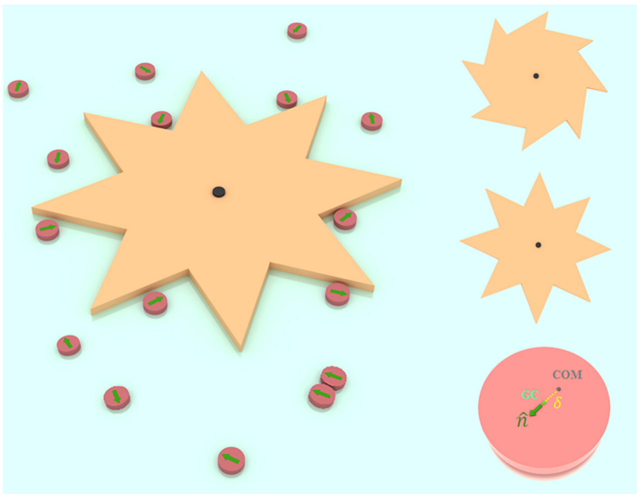

FIG. 1. Schematic diagram of a gear in the bath of self-propelling eccentric particles (SPEPs). Two kinds of gears with eight teeth of asymmetrical/symmetrical geometries are displayed. The gear is composed of 12 008 beads arranged along its perimeter with interval of 0.02 σ.The eccentric particle (disk) has a geometric center (GC, blue) and a center of mass (COM, gray) with a distance δ. The particle is self-driven along the orientation $\hat{\boldsymbol{n}}$, from COM to GC.

(COM). They displayed an amazing collective behavior in the small rotation-diffusion coefficient [17], due to the effective alignment caused by the mutual coupling of the positional and orientational degrees of freedom of each particle [18]. Inspired by the design of SPEPs, we raise two questions: Could gears rotate in the bath of active eccentric particles? And, what's the influence of eccentricity on the rotation behavior? Can it be used to optimize power output? To answer the questions, here we investigate the dynamics of gears with asymmetrical and symmetrical geometries in the bath of SPEPs via computer simulations. We find that the asymmetrical gear can rotate in a specific direction due to edge alignment of particles with corner trapping, with the angular speed first increasing and then decreasing as the eccentricity increases. Additionally, we found that the directional rotation of a symmetric gear depends on the particle-area fraction, the persistence length of motion, and the eccentricity, due to the existence of biased trapping with positive feedback. Eccentricity is not conducive to the rotation of a symmetric gear, but a small degree of eccentricity can help increase the angular speed of the gear. Moreover, we propose a machine-learning (ML) model to predict the angular speed for the asymmetric gear with the input parameters of particle-area fraction, eccentricity, and rotational-diffusion coefficient.

II. MODEL AND METHODS

The particle (disk) was modeled by a rigid body characterized by two centers (Fig. 1): one is the geometric center (GC), the other is the center of mass (COM) displaced from GC by a distance δ. A particle $\boldsymbol{i}$ is described by its GC $\boldsymbol{r_i(t)}$, COM $\boldsymbol{r_{ci}(t)}$, and orientation $\hat{\boldsymbol{n}}_{\boldsymbol{i}}(\boldsymbol{t})([\cos\theta_i, \sin\theta_i])$, which goes from COM to GC. All particles interact with an expanded Lennard-Jones potential with a distance shifted by Δ,

$$U(r_{ij}) = \begin{cases} 4\varepsilon\left[\left(\frac{\sigma}{r_{ij}-\Delta}\right)^{12} - \left(\frac{\sigma}{r_{ij}-\Delta}\right)^{6}\right] & r_{ij} < \Delta + \sqrt[6]{2}\sigma \\ 0 & \text{otherwise} \end{cases}, \tag{1}$$

where r_{ij} is the distance of GCs between particle i and j. It should be noticed that we also inspected the gear behavior without particle-particle interactions for comparison. Δ is the size of hard core.

The dynamics of each particle is described by the following equations:

$$m_c\ddot{\boldsymbol{r}}_{\boldsymbol{ci}}(t) = F_a\hat{\boldsymbol{n}}_{\boldsymbol{i}}(t) - \nabla_i U - \gamma_t\dot{\boldsymbol{r}}_{\boldsymbol{ci}}(t) + \sqrt{4\gamma_t k_B T_t}\boldsymbol{\eta}_{\boldsymbol{i}}(t), \tag{2}$$

$$I\,\ddot{\theta}_i\,(t) = \Gamma_i - \gamma_r\dot{\theta}_i(t) + \sqrt{2\gamma_r k_B T_r}\boldsymbol{\xi}_{\boldsymbol{i}}(\boldsymbol{t}), \tag{3}$$

$$\Gamma_i = \delta\;\hat{\boldsymbol{n}}_{\boldsymbol{i}} \otimes [-\nabla_i U], \tag{4}$$

where m_c is the mass of COM, I the moment of inertia, γ_t the translational-friction coefficient, γ_r the rotational-friction coefficient, F_a the strength of self-propelled force, k_B the Boltzmann constant, $U = \frac{1}{2}\sum_{i,j} U(r_{ij})$ the total potential of the system including active particles and beads on the gear. T_t and T_r are parameters of strength of translational and rotational noises, respectively. For the granular system, the $T_t = T_r$ is not mandatory. Γ_i denotes the torque on particle i due to collision. Besides, $\boldsymbol{\eta}_{\boldsymbol{i}}(t)$ and $\boldsymbol{\xi}_{\boldsymbol{i}}(\boldsymbol{t})$ are Gaussian white noises on the COM with zero mean and unit variances, as follows:

$$\langle\eta(t)\rangle = 0; \quad \langle\eta_\alpha(t)\eta_\beta(t')\rangle = \delta_{\alpha\beta}\delta(t-t'), \tag{5}$$

$$\langle\xi(t)\rangle = 0; \quad \langle\xi(t)\xi(t')\rangle = \delta(t-t'), \tag{6}$$

where η_α or η_β is the x/yth component of the vector $\boldsymbol{\eta}(\boldsymbol{t})$.

A symmetric gear or asymmetrical gear with eight teeth (Fig. 1) is placed in the center of box. The inner radii of the gear are set as 16σ for symmetric gear and 21σ for asymmetrical gear and outer radii of the gear are set as 30σ, respectively. The gear is composed of 12 008 beads arranged along its perimeter with interval of 0.02 σ; the interaction between the beads and the particles is a purely repulsive Weeks-Chandler-Anderson (WCA) potential as Eq. (1). We treat the gear as a rigid body. To focus on its rotational motion, we fix the position of its center but allow it to rotate freely [19,20]. The rotational motion of the gear is governed by

$$J\dot{\omega} = -\gamma_R\omega + \Gamma. \tag{7}$$

J is the moment of inertia of gear, γ_R the rotational-friction coefficient, $\Gamma = \sum_i \vec{r_i} \otimes \nabla_i U$ the total torque on the gear through collision by particles, and $\vec{r_i}$ the vector from the gear center to the ith bead.

Our model is two-dimensional with periodical boundary conditions in x and y directions. Initially, N particles were randomly placed in a square box of size L x L. m, σ, and ε are used as scaling units and the corresponding time unit $\tau = \sqrt{m\sigma^2/\varepsilon}$. The area fraction ϕ is defined as $\phi = \frac{N\pi\sigma^2}{4(L^2-A)}$, where A is the area of gear. We set $m_c = 1.1m$, $I = 0.01\,\mathrm{m}\sigma^2$, $k_B T_t = 0$, $k_B T_r = 0.1\varepsilon$, $J = 1\mathrm{m}\sigma^2$, $L = 50\sigma$, $\gamma_R = 100\sqrt{\varepsilon/m\sigma^2}$. In addition, we set $F_a = 100\varepsilon/\sigma$, $\boldsymbol{\Delta} = \sigma$, and $\gamma_t = 100\sqrt{m\varepsilon/\sigma^2}$,

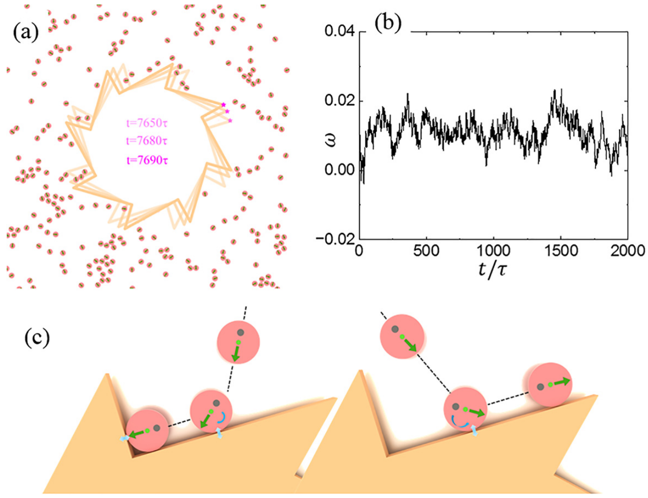

FIG. 2. (a) Snapshots at sequential times of the simulation, and (b) time sequences of angular speed ω for $\phi = 0.1$, $\delta = 0.1$, $D_r = 0.01$. (b) Schematics of collision of a SPEP from different incident angles.

γ_t and γ_R are large enough that the motions are essentially overdamped [19,20]. Keeping the inertial terms in Eqs. (2) and (7) allows us to use the velocity-Verlet algorithm. All simulations began from random initial configurations (Fig. 1). Particles with random orientation are placed homogenously in the box at the beginning. For each case, it ran in a minimum time of $1 \times 10^8\tau$ with a time step $10^{-4}\tau$. It should be pointed out that, since the radius of a SPEP is 1.0σ, δ in the range from 0 to 1σ can be used as the eccentricity of particles. It should be noted that the radius of particle is 2.0σ, which means that the largest eccentricity is 0.5 in our simulation. We mainly focus on the influence of particle-area fraction ϕ, eccentricity δ, and $D_r = \frac{k_B T_r}{\gamma_r}$, which controls the persistence length of a particle. Γ and angular speed ω were reduced by ε and $\frac{1}{\tau}$, respectively. Unless otherwise specified, the units of physical quantities in the following are the same as above.

III. RESULTS AND DISCUSSION

A. Asymmetrical gear

We first focus on the rotational behavior of the asymmetric gear in the bath of SPEPs with $\phi = 0.1$. A net unidirectional motion is observed, with a fluctuating angular velocity around a nonzero mean value. Typical snapshots for the time evolution of gear are given in Fig. 2(a), at $\delta = 0.1$. The instantaneous angular velocity of the gear as a function of time is shown in Fig. 2(b). The finding is in good agreement with previous work of an asymmetric gear in the bath of bacterial or Janus particles [10,12]. The onset of a directed rotation can be understood by analyzing the collision of a SPEP with the gear boundary [Fig. 2(c)]. When a SPEP touches a gear edge, it will exert a force on the gear. Meanwhile, the reacting force will produce a net torque to align the orientation of a SPEP along the edge. Depending on the incident angle, the SPEP will then dwell at the corner exerting a torque on the gear or leave the gear back. The mechanism applies for both the long and short edges. Most of the collisions will occur on the long edge and

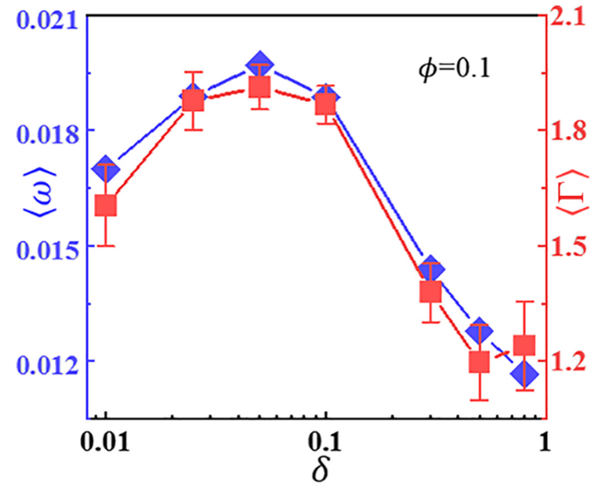

FIG. 3. Mean angular speed $\langle\omega\rangle$ and torque $\langle\Gamma\rangle$ as a function of eccentricity δ at $\phi = 0.1$, $D_r = 0.01$.

thus more SPEPs with orientation normal to the short edges. The mechanism is similar to that of rodlike particles such as bacteria [10].

Now, we turn to the effect of eccentricity on the mean angular speed $\langle\omega\rangle$. The method to extract $\langle\omega\rangle$s is given in Sec. I and Fig. S1 (Mean-square angular displacements as a function of time) of the Supplemental Material (SM) [21]. The $\langle\omega\rangle$ as a function of δ is plotted in Fig. 3. Interestingly, $\langle\omega\rangle$ increases and then decreases with δ, exhibiting a nonmonotonic behavior, implying that there is an optimal eccentricity for gear rotation. That is to say, eccentricity is indeed to be used as a parameter to adjust the angular speed. The profile of angular speed with the eccentricity is determined by the effective torque on the angular dynamics. To understand why there exists an optimal δ, we calculate the total torque exerting on the gear (Fig. 3). One can find that the torque shows the similar profile with $\langle\omega\rangle$ as the function of δ. The effective torque also first increases and then decreases with the increase of eccentricity. Intuitively, an increase of eccentricity strengthens SPEPs moving parallel to the gear edge, while it might promote cluster formation of SPEPs in the bulk, reducing the number of edge-clinging SPEPs due to steric interactions. We further investigate the system without pair-pair interactions among SPEPs and find a similar profile of $\langle\omega\rangle$ as a function of δ (see Fig. S2 for mean angular speed $\langle\omega\rangle$ and torque $\langle\Gamma\rangle$ as a function of eccentricity in the Supplemental Material [21]), indicating that the nonmonotonicity does not fully stem from density difference caused by interparticle interactions.

To further understand the nonmonotonicity of torque, we calculate the influx-particle number [Fig. 4(a)], dwelling time of each particle [Fig. 4(b)], and vertical component of active force [Fig. 4(c)] as a function of eccentricity for short and long edges, respectively, for the system without steric interactions between SPEPs. The influx-particle number is calculated by counting particle moving to the corner per τ. The dwelling time is the average time that a SPEP stays on the edges. One can find that, at each δ, influx-particle number is larger for the long edge and dwelling time is longer for short edge. These induce the larger force exerting on the short edge [Fig. 4(c)], which ensures the sustained unidirectional rotation. The

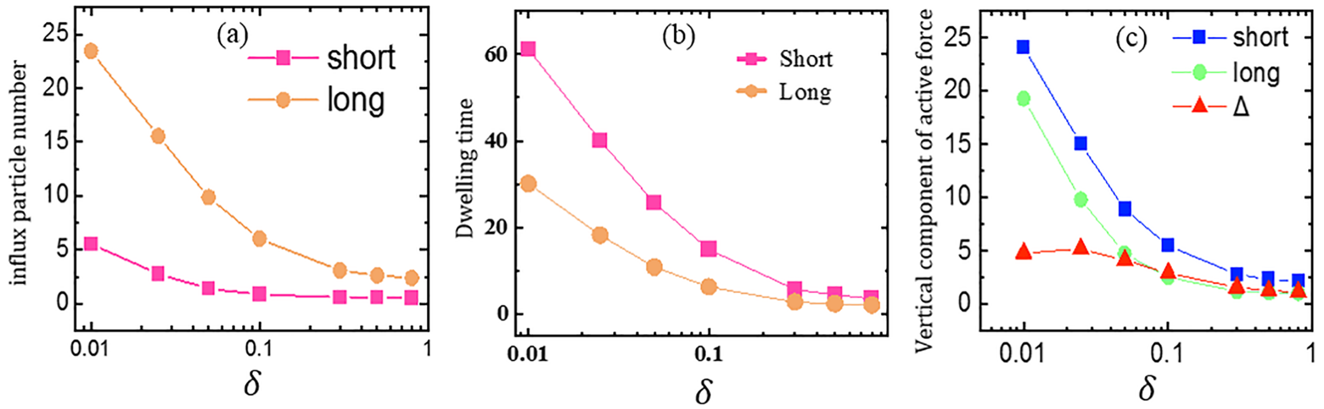

FIG. 4. The influx-particle number (a), dwelling time of each particle (b), and vertical component of active force (c) as a function of eccentricity for short and long edges, respectively, at $\phi = 0.1$, $D_r = 0.01$. Δsl denotes the difference of vertical component of active force applied to the short and long edges.

vertical components of active forces exerting on the short edge and the long edge decrease with the increase of eccentricity. However, the difference between them exhibits a profile of first increasing and then decreasing as a function of δ, which induces the nonmonotonic profile of $\langle\omega\rangle$.

$\langle\omega\rangle$ in the $\phi-\delta$ space is given in Fig. 5(a), which demonstrates that all $\langle\omega\rangle$s are larger than zero in our parameter window. It indicates that the asymmetric gear can directionally rotates in the bath of SPEPs. $\langle\omega\rangle$ also changes with the particle fraction at a specific δ. At $\delta = 0.01$, $\langle\omega\rangle$ slightly increases with ϕ, where a larger area fraction brings more particle close to the gear. At larger δs $(= 0.1$ and $0.5)$, it increases first then decrease with ϕ. This is because large fraction of SPEPs in the bulk promotes the cluster formation of SPEPs at larger δs (see Fig. S3 and Fig. S4 for typical snapshots in the Supplemental Material [21]), then lowers collision frequency of SPEPs with the gear. Here, ϕ is smaller than that $(\phi > 0.4)$ at which cluster forms for the system of active Brownian particles. [22]

B. Machine learning predicts the optimal value

How to obtain the optimized angular speed is another intriguing topic? Although extensive parameter scanning with high computational cost might achieve the goal, here we propose to explore the issue using a machine-learning approach. We employ the combined machine-learning (ML) methods of random forest regressor (RFR) [23] and Bayesian optimization (BO) [24] to train a model via supervised learning based on our simulation data and to predict the optimum ω. A brief introduction to these methods is given in the SM [21]. Figure 8(a) illustrates the process flow. The training process begins with input parameters—represented by D_r, δ, and ϕ —which serve as the model's independent variables. These input data are first used to train a random forest regressor, which learns the nonlinear relationships between the inputs and the target variable ω. To improve the model's performance, Bayesian optimization is employed to tune the hyperparameters of the random forest, ensuring that the model achieves the highest predictive accuracy. Once the optimized random forest model is obtained, differential evolution [25] is applied to search for the optimal combination of input parameters (D_r, δ, and ϕ) that maximizes the ω.

We use 80% of the data from the database as the training set for initial model construction, and then use the remaining 20% of the data as the test set to evaluate the model's predictive performance. Figure 6(b), as well as Tables S1 and S2 in the Supplemental Material [21], evaluates the predictive results of our model. Besides, the coefficient of determination (R^2) is

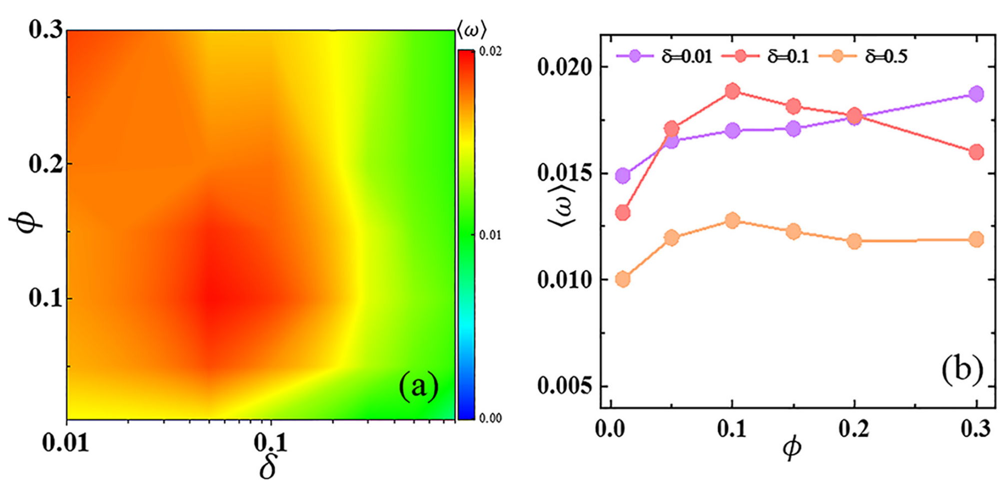

FIG. 5. (a) $\langle\omega\rangle$ in the ϕ-δ space. (b) $\langle\omega\rangle$ as a function of ϕ for various δs.

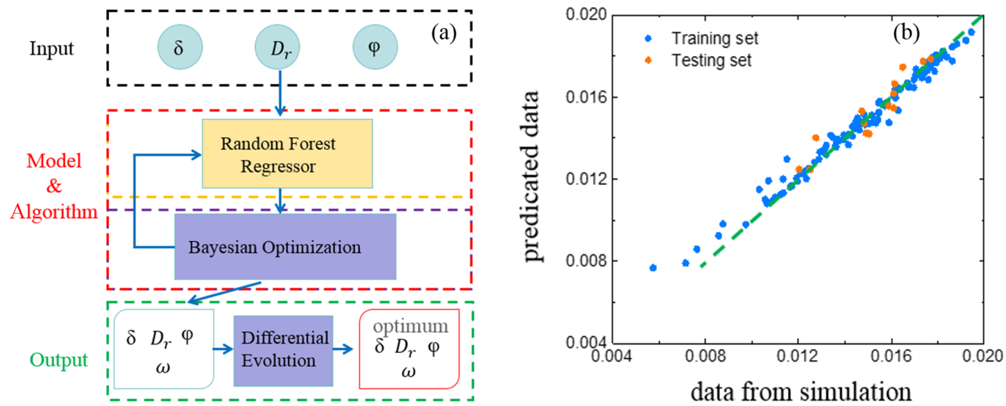

FIG. 6. (a) Flowchart of the process for predicting the optimum ω using the combination of random forest regressor and Bayesian optimization. (b) Comparison of the training and test ωs. The green line denotes $y = x$.

utilized to evaluate the goodness of fit (see Sec. II of the Supplemental Material [21]). Tenfold cross validation is used in our numerical experiments (see Table S1 of the Supplemental Material [21]). The average R^2 reaches to 0.91. It demonstrates the effective predictive capability of the ML model for ω. Through differential evolution method, we obtained the optimum value of $\omega = 0.019\,23$ at the features: $D_r = 0.000\,93$, $\delta = 0.034\,83$, and $\phi = 0.115\,15$. It should be noted that the ML model cannot provide an analytical function; however, the model can be used to predict ω under various variables and determine the maximum value of ω, which is not necessarily the peak value of Figs. 3 or 5.

C. Symmetrical gear

For symmetrical gear, we observed three states under different conditions. For example, at $\phi = 0.1$, $\delta = 0.05$, $D_r = 0.001$, unidirectional rotation exists, with the ω fluctuating around a nonzero mean value [Fig. 7(a)]; at $\phi = 0.15$, $\delta = 0.3$, $D_r = 0.001$, the gear could rotate in one direction for a long-time interval, but the direction could reverse many times due to sudden and large fluctuations [Fig. 7(b)]. In another state, the gear shows a random rotation without apparent directional rotation (data not shown). The unidirectional rotation significantly depends on the parameters ϕ, D_r, and δ. Phase diagram in the ϕ-D_r space at $\delta = 0.1$ is depicted in Fig. 7(c). It can be found that at large- and small-area fraction, the gear is hard to rotate directionally. It is also hard at large D_r. For large ϕ, particles aggregate in the bulk, which results in the decrease of particle density around the gear. Therefore, the phenomenon is similar to that of low-fraction system. We also give the phase diagram in the ϕ-δ space at $D_r = 0.001$ [Fig. 7(d)]. It can be found that the symmetric gear shows no directional rotation when $\delta > 0.3$. Directional rotation of symmetric gear occurs at specific parameters: small D_r, low δ, and mediate ϕ.

The narrow space of parameters for unidirectional rotation of symmetric gear is caused by the mechanism similar to that of ABPs, in the bath of which rotation of the gear happens in small D_r [13]. Because D_r is small, the rotation of particle with small δ is difficult, i.e., it needs a long time to change propelling direction. Thus, the behaviors of SPEPs after hitting the two sides of a rotating tooth are different (see Movie SI/II for typical trajectories of a SPEP hitting on the gear in the Supplemental Material [21]). We refer to these two sides as "head-on side" (HOS) and "rear-end side" (RES), respectively (see Fig. S5 for schematics of collision of a SPEP with the HoS and ReS in the Supplemental Material [21]). When an SPEP collides onto the HOS, it tends to slide inward in the next moment due to the rotation of the gear and is then trapped in the groove until the gear rotates by a large enough angle that the propelling direction on the SPEP becomes outward. In contrast, when a SPEP collides onto the RES, it tends to slide outward and leave the gear. The rotation of the gear and biased trapping on incident SPEPs form a positive-feedback loop that sustains the unidirectional rotation. It should be noted that this mechanism only works for small D_r. For large D_r, especially, when the time scale of gear rotation is larger than that of torque-induced particle rotation (i.e., SPEPs change direction easily), the mechanism (edge alignment with corner trapping) for asymmetric gear works and, hence, unidirectional rotation of symmetric gear disappears.

Now, we turn to mean angular speed as a function of eccentricity at $\phi = 0.1$, $D_r = 0.001$ (Fig. 8). The unidirectional rotation of symmetric gear critically depends on the D_r and δ. We find, at small δs, the $\langle\omega\rangle$ increases then decreases with δ. The finding is in good agreement with that for asymmetric gear. It implies that, at the small D_r and δ, the profile of $\langle\omega\rangle$ with δ is independent of geometric symmetry. For both symmetric and asymmetric gears, the biased trapping with positive-feedback mechanism exists at low eccentricity, leading to unidirectional rotation. At high eccentricity, the edge alignment with corner-trapping mechanism dominates in both cases as well; but the unidirectional rotation is determined by geometric asymmetry. For geometrically symmetric gears, unidirectional rotation disappears.

At the small D_r and δ, the $\langle\omega\rangle$ increases with δ is independent of geometric symmetry. It is because the biased trapping with positive-feedback mechanism dominates here, and δ enhances the torque-transfer efficiency. When $\tau_r = \frac{1}{D_r} \gtrsim \frac{2\pi}{\omega}$, i.e., the particle rotates slowly compared with the gear, the incident angle of a SPEP turns from acute to obtuse due to the gear's rotation [Fig. 8(b)]. Then the SPEP tends to slide inward; meanwhile, the eccentricity induces a torque, which facilitates the alignment of the particle's motion direction with

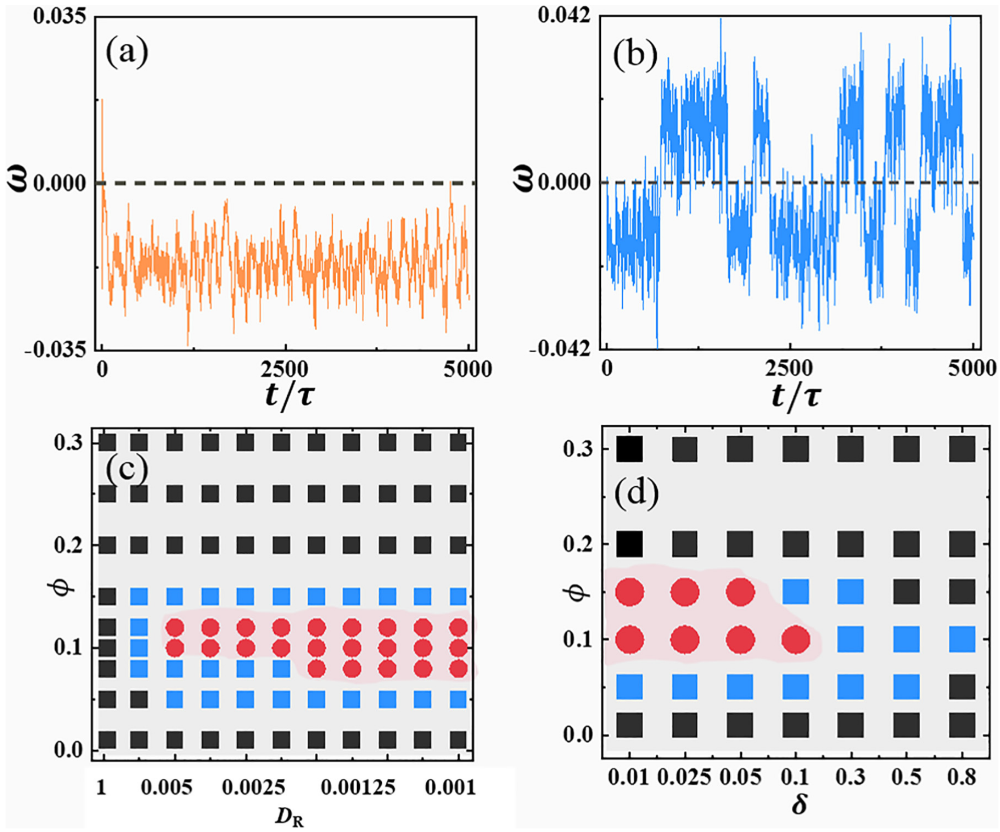

FIG. 7. (a) Time sequences of angular speed ω for $\phi = 0.1$, $\delta = 0.05$, $D_r = 0.001$. (b) Time sequences of angular speed ω for $\phi = 0.15$, $\delta = 0.3$, $D_r = 0.001$. Phase diagram in the ϕ-D_r space at $\delta = 0.1$ (c) and ϕ-δ space (d) at $D_r = 0.001$. Black squares, blue squares, and red circles represent the random rotation, reversable rotation, and unidirectional rotation, respectively. The colored backgrounds represent the nondirectional rotation (light grey) and unidirectional rotation (light red).

the boundary. An increase in δ further enhances this alignment, thereby accelerating the SPEP's approach to the corner. That's why the $\langle\omega\rangle$ increases with δ. It should be emphasized that the argument is valid when the incident angle is close to 90°. When the angle deviates significantly or δ is large, the induced torque will hinder the positive-feedback effect. The quantitative results are given in Fig. 8(c), which shows the probability that SPEPs move toward the corner after colliding with the gear for the system, that the gear rotates with a fixed $\omega = 0.015$, and there are no steric interactions between SPEPs. The results show that even when the incident angle deviates slightly from 90° (ranging from 70° to 90°), there

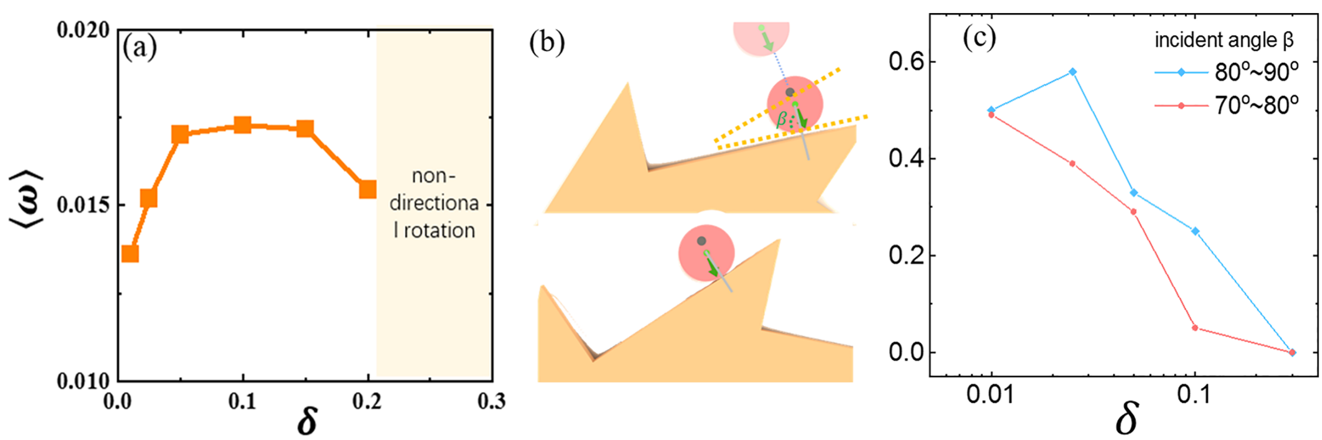

FIG. 8. (a) $\langle\omega\rangle$ as a function of δ at $\phi = 0.1$, $D_r = 0.001$. (b) Schematics of positive-feedback mechanism. The yellow dashed line is eye guiding for the gear boundaries. The incident angle β of the SPEP turns from acute to obtuse due to the gear's rotation. (c) The probability of SPEPs moving to the corner at the incident angles ranging from 70° to 90° for the system without steric interactions between SPEPs at the fixed $\omega = 0.015$.

remains a finite probability for SPEPs to move toward the corner, which approaches zero only when the $\delta \geqslant 0.3$. The profile of probability as a function of δ is similar to that of $\langle \omega \rangle$ when the incident angles range from 80° to 90°.

IV. DISCUSSION

The ratcheting effects of active matters have been studied quite intensively over the last few decades [26]. It was found that two ingredients are required to produce a ratchet effect: one is the running of active agents along the boundaries, and the other is the breaking of detailed balance by activity. The effect is reduced by a finite temperature and steric agent-agent interactions. The active-ratchet effect can be used to transport larger-scale asymmetric objects such as a gear [27–29]. Here, we introduce a new parameter, eccentricity, into disklike active particles for regulating the gear's rotation. Compared with active Brownian particles, the introduction of eccentricity induces an alignment effect. The effect is twofold: The collisions with the gear boundary generate an effective torque that contribute to the particle's motion along the periphery, reducing the time to reach the corner. Concurrently, the torque arising from persistent interparticle collisions favors velocity alignment, which in turn supports the development of collective motion [30,31]. Although rodlike particles also have the alignment effect, they tend to be trapped at corners and destroy the positive-feedback mechanism due to anisotropic interactions with gear boundary [10].

Our results demonstrate that the angular speed and rotation direction of the gear immersed in a bath of SPEPs are highly sensitive to the geometric and dynamic characteristics of both the gear and the active particles. Two rotation mechanisms were identified—edge alignment with corner trapping, and biased trapping with positive feedback—each dominating under different conditions of rotational diffusion and eccentricity. When D_r is small, particles maintain their orientation longer, enhancing the efficacy of both corner-trapping and biased-trapping mechanisms. In contrast, large D_r disrupts persistent motion and weakens the time correlations necessary for the feedback loop, especially in symmetric gears, effectively shutting down directed rotation. It is clear that gear rotation in active-particle baths is multiparameter dependent. Optimal performance arises from a careful balance between particle persistence, coupling strength (eccentricity), and bath density. Using the ML method is helpful to further achieve the goal. The present model can also be trained for the symmetric gear.

Another interesting topic is how to realize the system in experiment. A possibility is considering a foam gear in a bath of inertial vibrobots [32] designed in such a way that the geometric center of the particle does not coincide with the particle center of mass. Alternatively, the eccentric particle can be made of microrobot (Hexbug Nano) and a laser-cut circular foam plate [33] due to the heavy tail of Hexbug Nano. The possible designing parameters are listed in Table S3 of the Supplemental Material [21].

V. CONCLUSION

A gear in the bath of self-propelling eccentric particles is investigated by Brownian-dynamics simulation. Both asymmetric and symmetric gears are studied. We find that the asymmetrical gear can rotate in a specific direction, with the angular speed first increasing and then decreasing as the eccentricity increases. The rotation of the gear and biased trapping on incident SPEPs form a positive-feedback loop that sustains the unidirectional rotation and enhances the rotational speed at small eccentricity. Additionally, we found that the directional rotation of a symmetric gear depends on the particle-area fraction, the persistence length of motion, and the eccentricity. Eccentricity is not conducive to the rotation of a symmetric gear, but a small degree of eccentricity can help increase the angular speed of the gear. These findings open new directions for the design of active materials and micromachines [34–36], where optimal energy harvesting or mechanical control can be achieved through careful tuning of particle-level properties. To further achieve the goal, a machine-learning model is trained to predict the angular speed for the asymmetric gear, which might offer guidance to the experimental design.

ACKNOWLEDGMENTS

This work was supported by the National Natural Science Foundation of China (NSFC). W.-d.T. acknowledges financial support through an NSFC Grant No. 21674078. K.C. also acknowledges financial support from NSFC Grants No. 21774091 and No. 21574096. H.L. acknowledges financial support from an NSFC Grant No. 12204339.

DATA AVAILABILITY

The data that support the findings of this article are not publicly available. The data are available from the authors upon reasonable request.

[1] S. Anand, X. Ma, S. Guo, S. Martiniani, and X. Cheng, Transport and energetics of bacterial rectification, Proc. Natl. Acad. Sci. USA **121**, e2411608121 (2024).

[2] R. Di Leonardo, L. Angelani, D. Dell'Arciprete, G. Ruocco, V. Iebba, S. Schippa, M. P. Conte, F. Mecarini, F. De Angelis, and E. Di Fabrizio, Bacterial ratchet motors, Proc. Natl. Acad. Sci. USA **107**, 9541 (2010).

[3] A. Sokolov, M. M. Apodaca, B. A. Grzybowski, and I. S. Aranson, Swimming bacteria power microscopic gears, Proc. Natl. Acad. Sci. USA **107**, 969 (2010).

[4] X.-L. Wu and A. Libchaber, Particle diffusion in a quasi-two-dimensional bacterial bath, Phys. Rev. Lett. **84**, 3017 (2000).

[5] A. Solon and J. M. Horowitz, On the Einstein relation between mobility and diffusion coefficient in an active bath, J. Phys. A Math. Theor. **55**, 184002 (2022).

[6] L. Caprini, A. Ldov, R. K. Gupta, H. Ellenberg, R. Wittmann, H. Löwen, and C. Scholz, Emergent memory from tapping collisions in active granular matter, Commun. Phys. **7**, 52 (2024).

[7] A. Beyen, C. Maes, and J.-H. Pei, Coupling an elastic string to an active bath: The emergence of inverse damping, Phys. Rev. E **112**, L042103 (2025).
[8] M. C. L. Lugo, K. C. C. Bayer, S. G. Gonzales, and N. P. M., Confesor, λ -like transition in the dynamics of ratchet gears in active bath, Phys. Rev. E **102**, 052607 (2020).
[9] G. Xu and B. Ai, Rotation reversal of a ratchet gear powered by active particles, Soft Matter **17**, 7124 (2021).
[10] L. Angelani, R. Di Leonardo, and G. Ruocco, Self-starting micromotors in a bacterial bath, Phys. Rev. Lett. **102**, 048104 (2009).
[11] K.-W. Kim, Y. Choe, and Y. Baek, Symmetry-breaking motility of penetrable objects in active fluids, Phys. Rev. E **109**, 014614 (2024).
[12] C. Maggi, J. Simmchen, F. Saglimbeni, J. Katuri, M. Dipalo, F. De Angelis, S. Sanchez, and R. Di Leonardo, Self-assembly of micromachining systems powered by janus micromotors, Small **12**, 446 (2016).
[13] C. Wang, W. Lian, H. Li, W. Tian, and K. Chen, Spontaneous unidirectional rotation of a symmetric gear driven by spherical active particles, Natl. Sci. Open **3**, 20230066 (2024).
[14] J.-R. Li, W. Zhu, J.-J. Li, J.-C. Wu, and B.-Q. Ai, Chirality-induced directional rotation of a symmetric gear in a bath of chiral active particles, New J. Phys. **25**, 043031 (2023).
[15] X. Li and W. Zhu, Directed rotation of a symmetric gear driven by visual-perception-dependent particles, Chaos Solitons Fractals **190**, 115782 (2025).
[16] T. Xu, C. Qin, B. Tang, J. Gao, J. Zhou, K. Chen, T. H. Zhang, and W. Tian, Constrained motion of self-propelling eccentric disks linked by a spring, J. Chem. Phys. **161**, 064905 (2024).
[17] Y. Wang, Z. Shen, Y. Xia, G. Feng, and W. Tian, Phase separation and super diffusion of binary mixtures of active and passive particles, Chinese Phys. B **29**, 053103 (2020).
[18] T. Hiraiwa, Dynamic self-organization of idealized migrating cells by contact communication, Phys. Rev. Lett. **125**, 268104 (2020).
[19] H.-S. Li, C. Wang, W. Tian, Y.-Q. Ma, C. Xu, N. Zheng, and K. Chen, Spontaneous symmetry breaking induced unidirectional rotation of a chain-grafted colloidal particle in the active bath, Soft Matter **13**, 8031 (2017).
[20] C. Wang, H.-S. Li, Y.-Q. Ma, W. Tian, and K. Chen, Microrotor of a chain-grafted colloidal disk immersed in the active bath: The impact of particle concentration, grafting density, and chain rigidity, J. Chem. Phys. **149**, 164902 (2018).
[21] See Supplemental Material at http://link.aps.org/supplemental/10.1103/njcd-mc48 for the method for calculating the average angular velocity $\langle\omega\rangle$ and typical snapshots for the interplay of SPEPs and gear with steric interaction in Sec. I; the introduction of machine-learning algorithms including random forest, Bayesian optimization, differential evolution, and the cross validation of our model in Sec. II; and the description of supporting movies in Sec. III.
[22] Y. Fily and M. C. Marchetti, Athermal phase separation of self-propelled particles with no alignment, Phys. Rev. Lett. **108**, 235702 (2012).
[23] L. Breiman, Random forests, Machine Learning **45**, 5 (2001).
[24] D. R. Jones, M. Schonlau, and W. J. Welch, Efficient global optimization of expensive black-box functions, J. Glob. Optim. **13**, 455 (1998).
[25] R. Storn and K. Price, Differential evolution–a simple and efficient heuristic for global optimization over continuous spaces, J. Glob. Optim. **11**, 341 (1997).
[26] C. J. O. Reichhardt and C. Reichhardt, Ratchet effects in active matter systems, Annu. Rev. Condens. Matter Phys. **8**, 51 (2017).
[27] M. J. Y. Jerez, M. A. Bonachita, and M. N. P. Confesor, Dynamics of a ratchet gear powered by an active granular bath, Phys. Rev. E **101**, 022604 (2020).
[28] G.-J. Liao and S. H. L. Klapp, Clustering and phase separation of circle swimmers dispersed in a monolayer, Soft Matter **14**, 7873 (2018).
[29] M. Yang and M. Ripoll, A self-propelled thermophoretic microgear, Soft Matter **10**, 1006 (2014).
[30] P. Baconnier, O. Dauchot, V. Démery, G. Düring, S. Henkes, C. Huepe, and A. Shee, Self-aligning polar active matter, Rev. Mod. Phys. **97**, 015007 (2025).
[31] M. Musacchio, A. P. Antonov, H. Löwen, and L. Caprini, Self-alignment and anti-self-alignment suppress motility-induced phase separation in active systems, J. Chem. Phys. **162**, 244902 (2025).
[32] L. Caprini, D. Breoni, A. Ldov, C. Scholz, and H. Löwen, Dynamical clustering and wetting phenomena in inertial active matter, Commun Phys **7**, 343 (2024).
[33] J. Wang, T. Xu, J. He, K. Chen, and W. Tian, Transition from isotropic to polar state of self-driven eccentric disks, Chinese Phys. B **32**, 070501 (2023).
[34] F. Chen, Y. Zheng, W. Jian, Z. Li, J. Li, H. Li, Y. Wang, A. Mentbayeva, and W. Zhang, Graphitic hierarchical porous carbons derived from lignin-hydrogels for high-performance zinc-ion hybrid supercapacitors, J. Energy Storage **108**, 115163 (2025).
[35] D. Bekeshov, S. Ashimov, Y. Wang, and L. Wang, Understanding gas-enhanced methane recovery in graphene nanoslits via molecular simulations, Capillarity **6**, 1 (2023).
[36] W. Tian, Y. Wang, and Z. Toktarbay, Effect of surface grafting on the oil–water mixture passing through a nanoslit: A molecular dynamics simulation study, Adv. Compos. Hybrid Mater. **7**, 233 (2024).